LBL-12614

Lawrence Berkeley Laboratory
UNIVERSITY OF CALIFORNIA

Materials & Molecular
Research Division

Presented at the International Conference on
High Temperature Corrosion, San Diego, CA,
March 2-6, 1981

OXIDATION MECHANISMS FOR ALLOYS IN SINGLE OXIDANT GASES

D.P. Whittle

March 1981

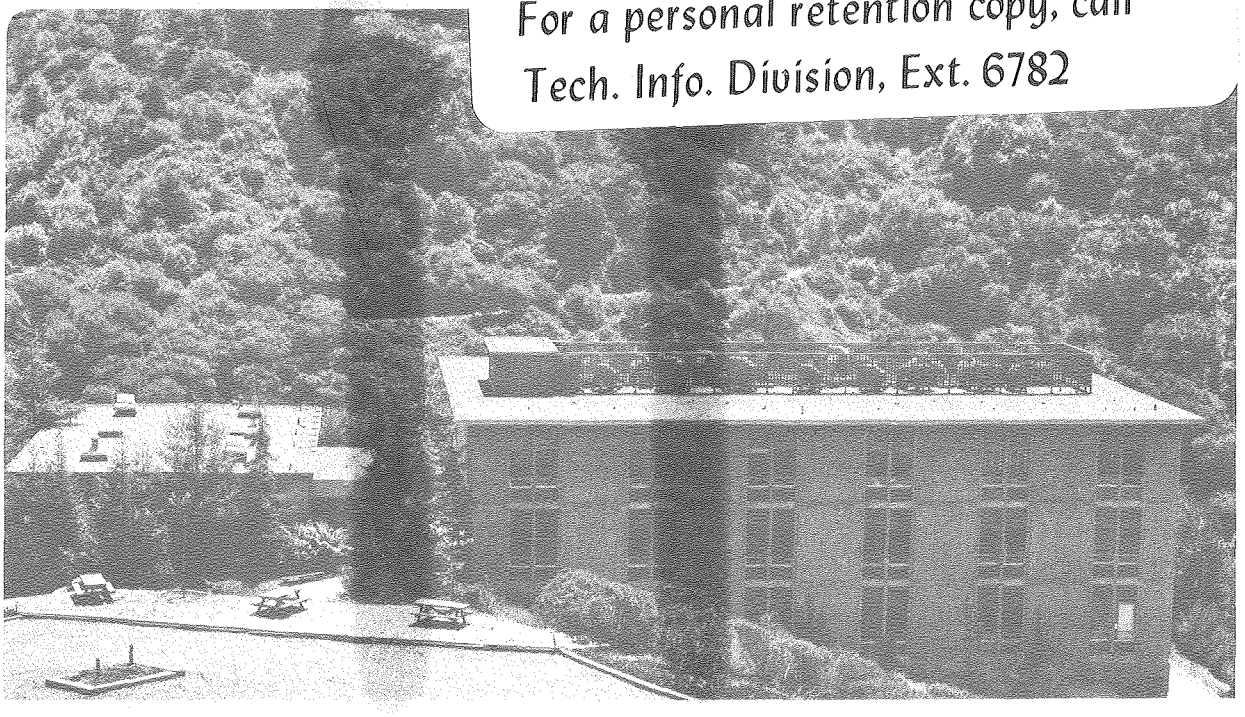

Prepared for the U.S. Department of Energy under Contract W-7405-ENG-48

DISCLAIMER

OXIDATION MECHANISMS FOR ALLOYS IN SINGLE OXIDANT GASES

D. P. Whittle

Department of Materials Science and Mineral Engineering
and Lawrence Berkeley Laboratory
University of California

Berkeley, CA. 94720

To be presented at the International Conference on "High Temperature Corrosion", San Diego, California on March 2-6, 1981.

ABSTRACT

Scales formed on alloys invariably contain the alloy constitutents in a ratio different from that in the alloy. In part, this is due to the differing thermodynamic tendencies of the alloy components to react with the oxidant, but equally it is due to differences in diffusion rates in scale and alloy phases. This complex "interrelationship" between transport rates and the thermodynamics of the alloy-oxidant system can be analyzed using multicomponent diffusion theory when transport-controlled growth of single or multi-layered scales occurs. In particular, the superimposition of the diffusion data on an isothermal section of the appropriate phase diagram indicates the likely morphologies of the reaction products, including the sequence of phases found in the scale, the occurrence of internal oxidation and the development of an irregular metal/scale interface. The scale morphologies on alloys are also time-dependent: there is an initial transient stage, a steady state period, and a final breakdown, the latter often related to mechanical influences such as scale adherence, spallation, thermal or mechanical stresses and void formation. Mechanical influences have a more devastating effect in alloy oxidation due to the changes in alloy surface composition during the steady state period.

INTRODUCTION

The field of alloy oxidation has widened considerably over the past 10-20 years, such that it is no longer possible to present a truly comprehensive review. The various monographs (1-4), review articles (5-7) and recent conference proceedings (8-11) provide much of the detailed observations of alloy oxidation behavior, and this review will attempt to characterize the different phenomena involved, and to identify important limiting cases which can be analyzed quantitatively, or at least semi-quantitatively. No attempt is made to cover equally all aspects of the subject here, or to provide a comprehensive reference list. Most of the examples used involve alloys based on Fe, Ni or Co, especially those containing Cr and/or Al, on which many commercial high temperature materials and coatings, particularly of the overlay type are based.

In almost all cases, especially those involving the practically important, oxidation-resistant alloys, a superficial scale forms on the surface of the alloy immediately upon exposure to the oxidizing gas, and all further reaction involves the transport of either the alloy components outwards or oxygen inwards, across the scale layer. Thus, the composition, structure and distribution of the phases in the scale layer are important. Transport rates through oxides depend on the defect structure, which is determined by composition, and on structural features such as grain boundaries, dislocation networks and other short circuit paths. In addition, however, the distribution of the phases - scale morphology - is also important. Unlike the scales formed on pure metals which have well defined layered morphologies, the extra degree of thermodynamic freedom permits the growth of two phase regions within the scale or alloy (internal oxidation) and/or the development of non-planar interfaces between adjacent phases. These features are determined, at least in part, by a complex interplay of thermodynamic and kinetic factors as will be discussed in a subsequent section. They are also time-dependent: as detailed in the next section, there is a transient oxidation stage, a steady state period and a final breakdown, the latter often related to mechanical influences such as scale adherence, spallation, thermal or mechanical stresses, void formation etc. These mechanical influences usually have a much more devastating effect in alloy oxidation than with pure metal oxidation, as will be shown later.

CHRONOLOGY OF ALLOY OXIDATION

Figure 1 shows schematically the three generally accepted stages in the oxidation of an alloy, noting that the imposed oxidation conditions - temperature, oxygen pressure, flow rate, etc. - are supposedly fixed. Upon initial exposure of the alloy, the oxides of essentially every reactive component are formed in a proportion given by the composition of the bulk alloy (12). Oxide nuclei with high intrinsic growth rates, for example NiO, CoO, FeO, Cu_2O, etc. overgrow the nuclei of the slower growing oxides, spinels, Cr_2O_3, Al_2O_3, etc. The rapid kinetics of the overgrowth formation contribute to a relatively high initial rate of oxidation. While the overgrowth is forming, the underlying nuclei of the slower growing, and usually more stable, oxides grow laterally. Eventually, they may impinge and form a continuous layer, or may remain as isolated precipitates in the faster growing matrix. This depends on the various factors which determine the steady state scale configuration.

Eventually, the transient oxidation period gives way to a steady state, which essentially means that the morphology in the scale is independent of time. Generally, the overall oxidation rate is governed by transport of one or more species through a particular layer in the scale and as a consequence will approximate to a parabolic rate law. This also implies, as will be seen later, that the interface compositions, and indeed the concentration profiles through the scale and alloy, when expressed as a function of $x/\sqrt{t}$, are independent of time. This steady state period is important practically. Any oxidation-resistant alloy depends on this period for continued protection. It cannot last indefinitely, since usually selective removal of one of the alloy components is taking place, and as a consequence, it must end at least when all that component has been removed from the alloy. The ultimate (equilibrium!) state of an alloy in oxidizing conditions is an oxide containing the alloy components in the same ratio as in the original alloy. Usually, the end of the steady state period occurs before all the selectively oxidized element has been consumed, by some type of mechanical disruption of the oxide scale. Then, because the alloy is a different composition than originally, it does not regain its steady state oxide.

Typical, schematic kinetic curves for the oxidation of an alloy are included in Figure 1. The duration of the steady state oxidation period is the critical factor in most applications of oxidation-resistant alloys.

The more severe the conditions, such as higher temperatures, rapid temperature cycles, simultaneous mechanical stress or erosion, and so on, the shorter it becomes.

STEADY STATE SCALE MORPHOLOGIES

Initially it is worthwhile to examine the factors which govern the scale morphology during the steady state before discussing the initial and final stages. Moreau and Benard (13) drew up a schematic classification according to the distribution of the phases in the scale and this was subsequently adopted by Wood (5) and Wallwork (7). More recently, Bastow et al. (14), by considering the elemental distributions through the scales, presented a more comprehensive classification, complementary to that of the diffusion path approach of Dalvi and Coates (15). This approach, with some simplification, is the one adopted here: for a more detailed description, reference to the original paper (14) is recommended.

A convenient starting point is the isothermal section of the alloy (binary, for convenience of representation) - oxygen system. More and more of these diagrams are becoming available (16), although, some care must be exercised in their selection. In some cases (17, 18) for example, the so-called 'equilibration' technique, where a given alloy is oxidized for a brief period and then the scale is equilibrated, does not produce a true equilibruim diagram.

Figure 2 shows a typical section through the Ni-Cr-O system at 1000^{o}C (15). Clearly three oxides are stable: NiO, Cr_2O_3 and $NiCr_2O_4$. All occupy an area on the diagram indicating mutual solubility, and a range of stoichiometry: complete immiscibility is unlikely. Consider what happens when an alloy, for example Ni-20Cr, point A is exposed to oxygen, O. The eventual product would be indicated by the point E, that is where the line joining the alloy composition to the oxygen corner contacts the oxide-oxygen three phase fields, that is would consist of a mixture of NiO and $NiCr_2O_4$ with the overall Ni:Cr ratio of 80:20 as in the original alloy. However, this is the eventual product. During most of the oxidation reaction, the reactants are separated from one another by the superficial scale and thus cannot immediately react to give the final product. The overall free energy change involved in the oxidation reaction is thus spread out over a large distance, although it is usual to invoke the concept of local equilibrium, such that any microscopic element is substantially at equilibrium with itself. This, of course,

also implies equilibrium at interfaces between various phases, although in this ternary system it is clear that this in itself is not sufficient to define the interface composition. For example, in the Ni-Cr-O system (Figure 2) any phase or mixture of phases appearing along the lower line bounding the oxide-oxygen gas phase fields could be in equilibrium with oxygen. This is, of course, in contrast to the case of a pure metal, when with one less degree of freedom, the composition (stoichiometry) of say NiO in equilibrium with a given PO_2 at constant temperature is fixed.

It is convenient then to trace out on to the phase diagram the locus of compositions (also called reaction path (6) or diffusion path (15,19, 20) which indicates the sequence of phases, or phase mixtures, present in the scale, starting from point 0, O_2 gas, and finishing with the point representing the alloy bulk composition (15). If the oxidation of the alloy has a steady state period, and the majority of alloys do, when the overall oxidation process is transport-controlled, then a single reaction path describes this time-independent scale morphology. Even if there is no steady state period, then the reaction path concept can still be used, but of course, its position and shape will vary during the progress of the oxidation reaction. Equally if local equilibrium at phase interfaces is not maintained, the reaction path will not be continuous between its two end compositions.

The principles governing the direction the reaction path takes on the phase diagram, and hence the resulting scale morphology, is subject to certain limitations (21), but can best be established by considering a number of limiting cases when most of the rules become apparent. Basically, these are four types of binary alloy-oxygen systems:

(a) Only one stable oxide (noble metal alloys),
(b) Complete miscibility between the two oxides,
(c) Partial miscibility between the two oxides (complete immiscibility is unlikely),
(d) Partial miscibility between the two oxides and formation of an additional compound oxide or oxides.

(a) and (b) represent, of course, somewhat simplified systems, but are important limiting cases: firstly, because they can be analyzed quantitatively and secondly, because many aspects of the more complex systems (c) and (d) approximate to (a) and (b) under limiting conditions.

(a) One Stable Oxide - Noble Metal Alloys

Figure 3 shows schematically the scale morphologies which can be produced relating these to the diffusion paths on typical phase and alloy - PO_2 diagrams. Probably, the simplest scale (a) which can be formed is that produced when the noble metal, A, is thermodynamically inert and a B(O) scale is formed as in the oxidation of pure B. The fundamental difference between the B(O) scale on a binary alloy and that on pure B metal is that scale formation in the former case must be associated with an enrichment of A in the underlying alloy. Scale growth can then be determined by the supply of B to the alloy-scale interface, as discussed theoretically by Wagner for the oxidation of Pt-Ni alloys (22). Other examples are found in the sulfidation of Co-Cr alloys (23) at low sulfur fugacities and Ni-Cr alloys at temperatures above 900^{o}C (24) when Cr is the base metal in both cases, Co and Ni remaining inert because their sulfides are unstable under the imposed conditions.

Two further types of morphology are possible with these noble metal alloys rich in the oxidizable component, depending principally on whether oxygen shows significant solubility in the alloy or not. If it does not, 3(b), then there is a tendency towards the development of an uneven alloy/scale interface and the incorporation of particles of noble metal into the scale. This has been examined theoretically by Wagner (25) although to date, only appears to be relevant to the sulfidation of Ag-Au alloys as studied originally, and perhaps more recently to the sulfidation of Ni-Cr alloys (24). Indeed, when the rather restrictive assumptions of Wagner's original model, namely negligible solubility of oxygen in the alloy and the more noble component in the oxide, were relaxed by Whittle et al. (26), it was shown that precipitation of B(O) internally behind the surface scale of the same phase was more likely to occur and relieve the supersaturation, 3(c). Wagner (27) also defined these conditions, with particular reference to Cu-Pt and Cu-Pd alloys.

At lower B (oxidizable element) contents in the alloy, B(O) is formed exclusively as an internal precipitate within the alloy matrix, 3(d). Ag-base alloys containing small concentrations of reactive elements and Cu or Ni-base alloys exposed at low oxygen

potentials are typical examples. The general subject of internal oxidation, with numerous examples, has been well reviewed by Rapp (28) and theoretical treatments relating the rate of penetration of internal oxide to the product of oxygen solubility and diffusivity are available (28). From a practical standpoint, probably the most important feature is the transition between internal oxidation and exclusive external oxidation, which, according to Wagner (29), occurs when a critical volume fraction of internal oxide precipitates at the reaction front. Rapp (30) tested this transition criterion in the oxidation of Ag-In alloys at 550°C; the transition corresponded to a volume fraction of 0.30 In_2O_3. However, the transition did depend on the initial surface treatment: a point to be emphasized later.

An alternative, but equivalent, viewpoint for the transition from external to internal oxidation involves the supply of the easily oxidizable element B to the alloy/scale interface, and this has been discussed in detail by Wagner (22),and more recently by Smeltzer and Whittle (31). These latter authors related the transition to the manner in which the diffusion path in the alloy contacted the oxygen solubility curve (cases (a) or (c) in Figure 3) stressing the importance of thermodynamic interaction between dissolved oxygen and the base component. This latter factor affects both the flux of oxygen into the alloy and the solubility curve. Indeed, the shape of the solubility curve, particularly the alloy composition with minimum oxygen solubility, may be much more significant than hitherto realized.

(b) Complete Oxide Solubility

When both components of the alloy are oxidized, and the resulting oxides are completely miscible, they both appear in the scale, where their relative proportions are determined by the oxidation potentials of A and B and their diffusion rates in the alloy and scale. Typical relationships between diffusion paths and scale morphologies are shown in Figure 4. A general treatment of scale growth for these conditions has been provided by Wagner (32), who pointed out that, unless the diffusivities of A and B cations are equal, their concen-

tration will vary across the scale, the distributions of A and B depending on their relative diffusivities (Figure 4). The effects of these factors on the concentration and distribution of B in the scale have been examined in detail (33). Two limiting cases can be identified, which correspond to minimum and maximum values of the scale growth rate. (In the example used, B, the more easily oxidizable component is also the faster diffusing cation in the scale, and as a consequence, increase in the concentration of B in the scale causes faster scaling rates; the opposite situation would exist when the more easily oxidizable element was the slower diffusing cation). When diffusion in the alloy is very slow in comparison with that in the scale, the overall ratio of A to B in the scale can be shown identical with the alloy (34). As a consequence, there is no selective oxidation, and the differing tendencies of the alloy components to oxidize, as expressed by $\delta(\Delta G)$ ($= \Delta G^{o}_{AO} - \Delta G^{o}_{BO} > 0$ since component B forms the more stable oxide), has no influence at all on the composition of the scale, or its growth rate. This is shown in Figure 5, curves 3 and 4, where the oxide growth rate, expressed as a ratio to that on pure B, is shown as a function of alloy composition, for two values of $\delta(\Delta G)$, 20.9 and 125.6 KJ/mol. The other limiting case corresponds to diffusion in the alloy being much faster than in the oxide, when the composition of the oxide, and hence the oxidation rate, is controlled by the degree of selective oxidation, $\delta(\Delta G)$. Curves 1 and 2, Figure 5, represent this case and at sufficiently large differences in stability of the component oxides, the oxide is virtually pure BO. Intermediate values of the ratio of diffusivities correspond to intermediate degrees of selectively oxidation and rates of oxidation. Corresponding concentration profiles through binary alloys of Co, Fe, Mn and Ni with one other, oxidized under most conditions of temperature and oxygen pressure, fall into this category, their oxides CoO, FeO, MnO and NiO all having a simple cubic, NaCl structure and forming solid solutions over their entire composition range. A single phase sulfide scale is also formed on Fe-Ni and Fe-Co alloys at low, <10 wt.%, Fe contents (35, 36). Alloy systems whose oxides have only limited miscibility, can also form single phase, solid solution scales, over certain composition ranges, for example dilute Ni-Cr and Co-Cr alloys, in which the solubility of Cr in NiO or CoO is

not exceeded (37) or chromium-rich alloys, when the oxide is Cr_2O_3 containing small concentrations of dissolved Ni or Co. The scales on some ternary oxidation-resistant alloys containing both Cr and Al also fall into this group, since the scale formed is essentially the solid solution Cr_2O_3-Al_2O_3.

One other case is indicated in Figure 4, which occurs when there is an usual dependence of cation diffusivities on oxide-composition. Mayer and Smeltzer (38) have shown that this is the case with Co-10% Fe alloys oxidized at oxygen potentials greater than 10^{-2} atm. and is consistent with the diffusivity of Fe^{++} ions in the (CoFe)0 being greater than that of Co^{++} ions at low oxygen potentials, and lower at higher oxygen potentials.

(c) Partial Miscibility of Component Oxides

Figure 6 shows a schematic section through a typical A-B-0 phase diagram in which oxides A0 and B0 are only partially miscible; B0 is the more stable oxide which is not evident from the phase diagram, but obvious (lower dissociation pressure) in the AB-PO_2 plot of Figure 6b. A crude classification of the oxides which can be stable in equilibrium with the alloy indicates (i) a releatively narrow composition range near pure A (ax) where "A0" (the quote marks indicating it is not necessarily pure) is stable; (ii) a relatively wide composition range (xb) where "B0" is stable and (iii) an intermediate composition (x) where "A0" and "B0" together are stable in contact with the alloy. Clearly, then the critical point is x, the alloy composition corresponding to the exchange reaction

'A0' + B = 'B0' + A

which is dependent on the difference in stabilities of the two oxides. Even in systems where the component oxides are not that different in stability, for example Cu-Ni, the point x lies close to the Cu (noble) side of the diagram: 0.4 at.% at 800°C (39). With more important practical alloys such as Fe, Ni or Co alloyed with Cr or Al, where the differences in stabilities is even greater (strictly speaking these belong to the next group of alloys since a mixed spinel phase $M_{1+x}Me_{2-x}O_4$ (M = Fe, Ni, Co; Me = Cr, Al) can also occur; however, analogously the appropriate exchange reaction to

consider is that between the two most stable oxides, 'Cr_2O_3' or 'Al_2O_3' and the spinel) then point x lies even closer to the A-rich side. Pettit (40) calculated $\sim 10^{-16}$ at.% Al for Ni-Al alloys at 900°C and Birks and Rickert (41) considerably less than 1 at.% Cr in Ni-Cr alloys at 1000°C. Croll and Wallwork (18) purported to have measured a value of 10 at.% Cr for the latter value, but the discrepancy is related to the manner of phase diagram determination, referred to earlier. Similar discrepancies between supposedly measured (17) values and those calculated (42) from thermodynamic data exist for the Fe-Cr system.

Although oxide 'BO' is more stable over virtually the entire composition range, whether it is able to form a continuous layer depends on the factors discussed earlier, namely the relative diffusion rates in alloy and scale. Thus, as an initial estimate, the criteria developed for noble metal alloys can be used. Thus, very approximately if 'BO' is a cubic (FeO,NiO, etc.) type oxide, only alloys containing about 50-70% B would show exclusive formation of 'BO'; for Cr_2O_3-type oxides the appropriate concentration is around 13-25% and for 'Al_2O_3', about 1-8%; however, although agreement in principle is good, there are many complicating factors.

Figure 6 also indicates that formation of 'AO' above is only possible over a very restricted composition range, and that simultaneous formation of the more stable 'BO' generally occurs, often as an internal oxide, which can subsequently dissolve not necessarily completely, upon subsequent incorporation into the surface 'AO' scale. Thus, if the alloy does not contain sufficient of the selectively oxidizable element to form a continuous layers of the more stable oxide, a two-phase scale results. As indicated earlier, Bastow et al. (14) have given a comprehensive description of the various possible scale morphologies, but generally the nature and distribution of the phases are difficult to define from first principles. It suffices to say here that alloys which do not develop a continuous layer of a single phase oxide are not usually important as practical oxidation-resistant materials.

(d) Formation of Compound Oxides

Transport of cations in a number of spinel phases is quite slow(43) and it might, therefore, seem attractive to attempt to develop alloys capable of forming scales of such compound oxides. However, the

rather restrictive conditions referred to above, and discussed in detail by Schmalzreid (44), make it extremely unlikely that a continuous layer of spinel, at least those of relatively narrow composition range, such as $NiCr_2O_4$, could be formed in a growing scale. Where the stability range of the spinel is greater, as for example in $Fe_{1+x}Cr_{2-x}O_4$, then of course the ionic transport rates through it, are correspondingly increased.

TRANSPORT IN SOLID SOLUTION OXIDES

Alloy oxidation phenomena are invariably associated with the growth of oxide solutions containing more than one cation, as has been adequately demonstrated in the previous section. Thus, it is clearly of major importance to understand how the transport properties vary with oxide composition. Mass transport proceeds primarily via defects, and the chemistry and physics of these imperfections in pure metal oxides have been intensively treated by Kofstad (45). In the case of oxide solutions, when the cations are of differing valencies, which usually also implies that the intersolubility is fairly limited, and deviations from the stoichiometric formula are small, the Wagner-Hauffe rules are mostly relevant. Electroneutrality is maintained by a redistribution of electronic and ionic defects, and thus for example in NiO, dissolution of Cr^{3+} ions increases the concentration or activity of cation vacancies but decreases the concentration of p-type defects. However, the over-optimistic application of these rules has led to disappointment in their lack of generality. This lack of agreement can usually be traced to: (a) the unrealized assumption that the oxide composition is uniform through the scale; that, is equal diffusion rates of the two cations - a rare occurrence, and (b) that the simple model of randomly dispersed, non-interacting point defects truly describes the non-stoichiometry of the oxide. Increasingly it is becoming clear (46, 47) that association between point defects can occur, even to the extend of formation of vacancy clusters (48, 49).

In oxide solutions in which the cations have the same valence, the Wagner-Hauffe rules do not apply. However, defect concentrations and hence the cation transport rates are still expected to vary with composition. In the cubic oxides, FeO, NiO, MnO, CoO, MgO, on the basis of a simple defect model involving only divalent cation vacancies, it has

been suggested (50)that in oxide solutions, for example, NiO-CoO, the free energy of formation of the vacancies according to

$$\tfrac{1}{2}O_2 = O^x + V_M^{z'} + zh^{\cdot} \quad (z = 0,1,2) \qquad (1)$$

is a composition weighted function of that in the two pure oxides

$$\Delta G^o_{V^{z'}} = (1 - \xi)\ (\Delta G^o_{V^{z'}})_{NiO} + \xi(\Delta G^o_{V^{z'}})_{CoO} \qquad (2)$$

where ξ is the equivalent fraction of CoO (the more stable oxide) in the solution. Using the electroneutrality condition this enable the cation vacancy concentration to be expressed as a function of oxide composition, and oxygen activity, by

$$[V^{z'}] = [V^{z'}]^o_{CoO}\ \beta^{\xi-1}\ a_0^{\frac{1}{2}(1+z)} \qquad (3)$$

where $[V^{z'}]^o_{CoO}$ is the mole fraction of vacancies in pure CoO at 1 atm. O_2 pressure, β is the ratio of the mole fraction of vacancies in pure CoO to that in pure NiO at 1 atm. O_2 pressure, a_0 is the oxygen activity. The cation diffusion coefficients in the oxide solution thus show an exponential dependence on composition:

$$D_{Co} = D^o_{Co}\ \beta^{\xi-1}\ a_0^{\frac{1}{2}(1+z)} \quad \text{and} \quad D_{Ni} = pD^o_{Co}\ \beta^{\xi-1}\ a_0^{\frac{1}{2}(1+z)} \qquad (4)$$

expressions verified experimentally in a number of cubic oxide solutions (51, 52). D^o_{Co} is the self diffusion coefficient of Co ions in CoO at 1 atmos. pressure, and p is the ratio D_{Co}/D_{Ni} assumed independent of compostions.

These expressions, equation (4), have been used in solving Wagner's (32) transport equation for the growth of solid solution scales, after some modification (50). Figure 7 shows the excellent agreement between experimentally measured concentration profiles and oxidation rate constants (53) for the oxidation of Ni-Co alloys and the same parameters calculated (50) using independently measured diffusion data. Similar agreement has been found for systems Ni-Co (54,55), Ni-Fe (56) and Co-Fe (57,58) alloys and for sulfide scales on Fe-Ni (59) and Fe-Co (60,61) alloys, although in some of these cases the data used for the calculation were not independently determined. Recent work with pure CoO (62,63), for example, indicates that the excess charge on the vacancies depends on the oxygen potential, and this has been incorporated into recent calculations (64,65) using available data for pure NiO (66,67) and CoO (62). In addition, some variation of the ratio of cation diffusivities can be accounted for (68), by incorporating the suggestion (69) that

correlation effects between the elementary vacancy jumps occur. Thus, even though the ratio of elementary jump frequencies for the two cations may be constant, the ratio of cation diffusivities varies with composition. Even this, however, never predits a reversal in the ratio of cation diffusivities, as observed in (CoFe)O solutions (38) and further work must be directed at the importance of vacancy aggregates, or clusters on transport in oxide solutions. Smeltzer et al. (70) have adopted an alternative approach, arbitrarily varying the parameters in eqn. (4) in order to improve agreement between calculated and measured concentration profiles and rate constants.

APPLICATION TO OXIDATION-RESISTANT ALLOYS

The oxidation of Fe, Co and Ni-base alloys has received a vast amount of attention and it is only intended to examine specific points here, which are amenable to a semi-quantitative discussion. Thus, remarks are restricted to Cr-containing alloys since, although the variation of oxidation-rate of Al-containing alloys with composition can be interpreted in a similar manner, quantitative information on diffusion rates in the relevant phases is largely unavailable. The experimental variation of oxidation rate with alloy composition, shown in Figure 8 (71), can be divided into four stages: (i) small additions (<1% or so) of Cr cause an increase in oxidation rate due to an increase in cation diffusivities in the appropriate cubic oxide MO. This increase can be described quantitatively (33) for dilute Ni-Cr alloys using the type of analysis referred to in the previous section. Moreover, because the concentration of native cation defects increases in the order NiO<CoO<FeO, there is a progressively decreasing probability of Cr-doping producing a sufficiently large increase in the total vacancy concentration to be totally consistent with the observed increase in oxidation rate. Other factors, such as internal oxidation and dissociative transport, may be responsible for the observed increases in such cases. (ii) When the solubility limit for Cr in the noble metal oxide is exceeded, a new spinel phase can be precipitated. This corresponds approximately to a maximum oxidation rate although other factors mentioned above and discussed elsewhere (71) cause the maximum to persist over different concentration ranges in various alloy systems. Thus, in Ni-Cr alloys the rate is virtually constant between 1 and 10 wt.% Cr because $NiCr_2O_4$ forms small, discrete precipitates which do not interfere markedly with cation diffusion in the NiO matrix. The spinel

in the Co-Cr system has a wider stability range, $Co_{1.3}Cr_{1.7}O_4$ - $CoCr_2O_4$, which permits precipitate growth sufficently to cause at least partial blocking of diffusion in the CoO matrix, thus preventing a constant maximum value of oxidation rate as the Cr content increases. As with Ni-Cr alloys, though, other factors are also involved. The extreme case, where the spinel has a sufficiently wide stability range to permit the eventual formation of a continuous blocking layer occurs in the Fe-Cr system where the phase $Fe_{1+n}Cr_{2-n}O_4$ ($0 \leq n \leq 2$) is formed. This occurs on alloys containing less than 1% Cr; the increase in oxidation rate caused by changes in the properties of FeO noted above, is terminated when spinel particles are precipitated in the FeO layer next to the alloy and a complete spinel layer is ultimately formed at this location, in agreement with the relative diffusion rates of Cr and Fe in Fe_3O_4 (72). While diffusivities have not been measured in the Cr-containing spinel, a comparison of the relative rates in FeO and Fe_3O_4 shows that cation diffusion in the latter is much slower. Consequently, the formation of a continuous spinel layer causes a sharp decrease in the oxidation rate immediately after the maximum is reached, as observed experimentally.
(iii) The detailed relation of oxidation rate to Cr content and the composition range over which the rate exceeds that for the pure noble metal component varies between different alloy systems (71) but in each case the upper Cr limit of this range is marked by a sharp decrease in rate. As noted above for Fe-Cr alloys, the initial decrease is associated with the formation of an inner layer of the spinel $Fe_{1+n}Cr_{2-n}O_4$. A further increase in the alloy Cr content eliminates FeO from the scale completely. At higher Cr contents the spinel phase is rendered thermodynamically unstable and this layer disappears also and for alloys still richer in Cr, the scale consists soley of the sesqui-oxide $(Cr, Fe)_2O_3$. Cation diffusivities, and consequently oxidation rates decrease rapidly in these compounds in the same order as they replace each other as the major phase in the scale. However, the actual growth rates of the sesqui-oxide scales are much greater than those predicted from diffusivities measured in single crystals, presumably due to short circuit diffusion effects. The Fe contents of these scales are small, typically $\sim$ 1%, because of the very strong selective oxidation of Cr and the relatively fast diffusion rates in the alloy ($D_{ferrite} \approx 100\ D^{Cr}_{Cr_2O_3}$), as discussed earlier.

The analogous sudden decrease in oxidation rate for Ni-Cr and Co-Cr alloys could also, in principle, be related to the eventual formation of a continuous spinel blocking layer in the matrix of the cubic oxide formed

originally. This is consistent with the fact that the ratio of the minimum alloy oxidation rate to that of the pure metal is approximately the same as the ratio of cation diffusivities in the spinel and the cubic oxide. Values at 1000°C are shown in the Table below along with the ratios for other significant scale compositions.

TABLE Comparison of Oxidation Rate Constants and Cation Diffusivities for Scales on Cr-Containing Binary Alloys

Alloy	Scale	K_p^{alloy}/K_p^{metal}	$\tilde{D}^{scale}/D^{MeO}$
Co-Cr	spinel (min. Kp)	1.1×10^{-4}	$5.1\text{-}5.7 \times 10^{-4}$
	'Cr_2O_3'	6.7×10^{-3}	1.3×10^{-3}
Ni-Cr	'NiO'	7.4	16
	spinel (min. Kp)	1.7×10^{-2}	$3.1\text{-}6.1 \times 10^{-2}$
	'Cr_2O_3'	0.82	2.25

However, in spite of these numerical similarities, there are no experimental observations of a spinel layer in the Ni-Cr system and, while there is some evidence for a rate-controlling layer in the Co-Cr system, this is limited to a very narrow alloy composition range. There is, moreover, considerable alternative evidence for a doped Cr_2O_3 scale when the oxidation rate is a minimum, as for Fe-Cr alloys. (iv) The value of oxidation rate increases from the minimum towards the value for Cr_2O_3 formation on pure Cr. For Fe-Cr alloys this increase is qualitatively consistent with the measured increase in cation diffusivities as the Fe content of $(Cr, Fe)_2O_3$ decreases, e.g. at 1273 $D^{Fe}_{Fe_2O_3} \approx 0.005\ D^{Cr}_{Cr_2O_3}$. In other alloys it has been associated with a comparable decrease in the doping effect as the concentration of Ni^{2+} or Co^{2+} in Cr_2O_3 decreases. However, the diffusivity measurements required to confirm these speculations have not been made at present and the implications of short circuit diffusion in the scales must always be considered.

THE INITIAL TRANSIENT STAGE OF OXIDATION

Most of the discussion so far has referred to the steady state scaling behavior of alloys, however, in many systems it requires time and considerable

thickness of scale before the steady state morphology is set up. This is particularly the case where more than one oxide phase can be formed. Transient effects when the oxide scale is a solid solution of the component oxides are not usually considered although undoubtedly it does take time for the concentration profiles to be established. Experimentally determined concentration profiles in the (Ni-Co)0 oxide formed at 1000^{o}C for periods from 1h up to 50 h, when plotted on a time-independent distance scale (ratio of distance from alloy/scale interface to total scale thickness) are coincident (50).

Transient effects are also not of major significance when only a single oxide is capable of forming - noble metal alloys - except for alloys near to the borderline between the transition from internal and external oxidation. This transition can rarely be assigned to a precise alloy composition, but over a range of compositions, Alloys within this range will show continuous oxide formation over parts of the surface and not over others. This is presumably related to slightly different rates of diffusion in differently orientated alloy grains, preferential diffusion paths in the alloy such as grain boundaries and other incoherent interfaces (73), temperature fluctuations, and so on.

Nevertheless, the most important transient effects are observed in systems in which more than one oxide phase can form, and particularly in alloys where the establishment of a continuous layer of a slowly growing, protective oxide is involved. A quantitative treatment of transient oxidation phenomena seems unattainable at present, but experimental studies in pseudo-model systems Cu-Ni (12) and Cu-Zn (74) and other systems (75) indicate that the continuous layer develops either by the lateral growth of the original surface nuclei of the more stable oxide, or by the impingement and coalescence of internal oxide particles within the alloy. Oxygen solubility and diffusivity in the alloy presumably determine the relative contributions of these two processes: growth rates of the component oxides are also critical, since these govern overgrowth and undercutting mechanisms.

The oxidizing conditions, particularly temperature and oxygen partial pressure, as well as the manner in which a sample or component is introduced to the oxidizing environment are also important parameters. This latter factor makes experimental studies difficult. By its very nature, the transient oxidation stage is completed very quickly, and attempts to modify the oxidizing conditions, lower temperature and oxygen partial

pressures, to slow down the process in order to study it more easily, only result in drastically altering the characteristics. High resolution techniques are usually also required, since the individual oxide nuclei are rather small. However, again the use of thin foil, transmission electron microscopy techniques again alter the characteristics of the transition, since there is not the reservoir of selectively oxidized element upon which to draw. In-situ scanning microscopy studies (76) may provide much of the answer.

The alloy interdiffusion rate is undoubtedly important in these early stages of oxidation when the protective scale is developing, determining how rapidly the preferentially oxidizing component can be replenished. Surface finish can also be involved. Giggins and Pettit (77) have shown, for example, that Cr_2O_3 develops on Ni-Cr alloys more readily over alloy grain boundaries than over the bulk of the grains, and on cold-worked surfaces than on polished ones. Equally, more nickel-rich oxides are formed on metallographically polished samples of TDNiCr than in samples which had been mechanically ground (78). However, an overriding feature is probably the presence of additional components in the alloy. Two types are important: additions of elements which form an oxide intermediate in stability between those of the eventual protective oxide and the noble metal, and additions of small concentrations (< 1 wt.%) of elements of very high oxide stability. Cu-Zn-Al (79) are the classical example of the first type where the presence of Zn helps establish an Al_2O_3 scale at considerably lower Al contents than in binary Cu-Al alloys. The classical explanation (79) is that ZnO predominates over Cu_2O in the initially nucleated scale and the ZnO provides a much lower oxygen potential to diffuse into the alloy allowing the Al to diffuse up to the surface and provide the healing Al_2O_3 layer immediately beneath the thin, initially, nucleated scale. Pickering (80) made a detailed analysis of this mechanism for the Ag-Zn-Al system. At 550^{o}C Ag-3% Al showed internal oxidation of the Al; Ag-6% Al exhibited partial formation of a protective external Al_2O_3 layer, and Ag-10% Al formed a continuous protective scale. However, Ag-21% Zn - 3% Al also exhibited a complete external protective Al_2O_3 scale.

Explanations along similar lines are usually put forward for the development of Al_2O_3 scales on Fe-Cr-Al, Ni-Cr-Al and Co-Cr-Al alloys (81-83) although other factors are surely involved (75). In all three systems, although as much as 20-30 at. % Al is required in the binary alloys to form Al_2O_3 (84), with around 15% Cr present, the amount of Al required becomes as low as 5 at.%: the effect is similar in the other two systems.

Other possibilities have been suggested (85) to explain the synergistic effect when two competing selectively oxidizable components are present in the alloy, since the amount of Cr required to act as a secondary getter would not be sufficient to form a continuous Cr_2O_3 external scale in the absence of Al, and this appears to be a requirement of the Wagner hypothesis. One possibility was that the presence of the third element (Cr) enhanced the diffusion rate of the other (Al): however, measurements of the off-diagonal diffusion coefficients in the diffusion coefficient matrix in Ni-Cr-Al (86) and Co-Cr-Al (87) alloys appear to negate this idea. The other possibility is that initially the Al oxidizes internally to form a dispersion of Al_2O_3 particles and these then promote the formation of a Cr_2O_3 scale, in the manner described below. The continuous Cr_2O_3 layer lowers the oxygen potential at the surface to the point where Al can diffuse outwards to develop a continuous Al_2O_3, beneath the Cr_2O_3 layer.

The second type of addition which has a major effect on the development of protective oxide scales is that of a small concentration of a very reactive element, typically Y, Hf, Ce, or of a fine dispersion of a very stable oxide: the effects of either addition are somewhat indistinguishable. The 'rare earth effect', as it has become known is made up of a number of factors, of which the one pertinent to the present discussion is the enhancement of selective oxidation of the protective scale-forming element, particularly during the early stages of exposure. Other aspects of the 'rare earth effect', have been reviewed recently (88).

Whittle et al. (89) oxidized Co-15% Cr alloys containing 1% additions of Hf, Zr or Ti without observing any effect on the overall oxidation rate. The scale formed was similar to that on a binary Co-15% Cr alloy: an outer layer of CoO and an inner CoO layer containing dispersed particles of the spinel and sesquioxides. However, if the active element additions were first converted to an oxide dispersion by an internal oxidation pretreatment (this was accomplished by sealing samples in capsule containing a Rhines pack, Cr + Cr_2O_3 powder mixture) then on subsequent oxidation a continuous Cr_2O_3 was able to develop on the surface. Thus, the presence of the oxide dispersion reduced the Cr concentration in the alloy necessary for continuous Cr_2O_3 formation from greater than 25% in the binary alloy, to less than 15%. Similar, but less dramatic, effects have been formed for Ni-Cr (90) and Fe-Cr (91) alloys. With alloys already containing sufficient Cr or Al to form continuous layers of Cr_2O_3 or Al_2O_3, the presences of an oxide dispersion markedly reduces the transient oxidation stage and reduces the amount of Ni-rich oxides formed on Ni-Cr alloys (92)

or Co-rich oxides on Co-Cr-Al alloys (93) for example. The model used to explain this behavior is summarized for a Ni-20 Cr alloy with and without a 2 vol.% ThO_2 addition, in Figure 9 (93). Essentially, the dispersed particles in the alloy surface act as nucleation sites for the first formed oxide, thus decreasing the internuclei spacing. The dispersoid represents a surface discontinuity, and it is not necessary to postulate that it preferentially acts as nucleation sites for Cr_2O_3 (or Al_2O_3). By decreasing the distance between adjacent Cr_2O_3 (or Al_2O_3) nuclei, the time required for the lateral growth process to form a complete layer of that oxide and terminate the formation of noble metal oxides is reduced. Direct experimental evidence for this model is difficult to obtain: the grain size of the oxide over the dispersion-containing material has been found to be between five and ten times smaller than over dispersion-free material, in accord with the model (92, 94). Furthermore, Flower and Wilcox (95) using in-situ oxidation of TDNiCr (Ni-20Cr-2ThO_2) in a high voltage microscope, showed some evidence that ThO_2 particles acted as preferential sites for oxidation. However, metal grain boundaries, slip steps and other inclusions were equally effective.

BREAKDOWN OF STEADY STATE SCALE MORPHOLOGY

Earlier sections have discussed typical steady state scale morphologies and how these are initially established, depending on the transport properties and interphase equilibria of the phases involved. As pointed out earlier, however, that steady state scale growth cannot continue indefinitely since one alloy component is usually been selectively oxidized out of the alloy. Whittle (96) has calculated the time of ultimate breakthrough, which is related to the scale growth rate, alloy interdiffusion rate and the thickness of the sample or component being oxidized. Calculated data approximately agree with experimental data generated during studies of the oxidation of stainless steel foils (97). More usually, however, other factors interrupt the steady state scaling pattern, resulting in more complex, sometimes localized, morphologies. Some of these possibilities are discussed below.

As oxidation proceeds the alloy is consumed and, if alloy-scale adhesion is poor, a gap can be formed between the alloy and scale, without scale fracture occurring, if the scale is sufficiently plastic. Alternatively, as suggested (98) for some Fe-Cr-Al alloys, a localized gap can be formed by a mechanism involving combination of the

scale components within the scale, rather than at either the outer or inner surface, causing the scale to grow away from the alloy. Isolation of the scale from the alloy, without suppression of the driving force for continued outward movement of cations, leads to the development of porosity in the inner regions of single layer scales and the disappearance of the inner, relatively cation-rich phases in multi-layer scales, with the continued growth of the outer, oxidant-rich, phases, as found, for example, during the sulphidation of Cu-Ni alloys (94).

When scale fracture occurs the oxidizing atmosphere can gain access to the underlying alloy which has, very probably been denuded of the less noble metal. If the less noble metal content is insufficient to ensure the re-establishment of the original scale (100) a completely new oxidation reaction can ensue at each fracture site, with the scale incorporating relatively much larger fractions of the more noble alloy components than those in the original scale, as is well known from extensive research on the breakaway oxidation of heat resistant alloys. Morphologies in such cases can become very complex, and highly localized, since re-oxidation is not determined by uniform outward growth but includes a lateral contribution, drawing oxidizable cations from alloy regions beneath the existing adherent scale. In addition, compressive stresses, caused by the formation of new oxidation products which are less dense than the original scale, might cause further fracture.

Transport of either metal cations or oxidizing species along preferential paths through scales such as grain boundaries, cracks and pores must obviously lead to deviations from morphologies based on uniform one-dimensional transport. Depending on the species preferentially transported, the possibilities include the non-uniform precipitation of a second phase within the scale and scale growth at preferred sites, causing the build-up of stress, followed by scale fracture, with the consequences noted earlier. Non-uniform internal oxidation of the alloy can also occur for similar reasons (73).

The fact that porosity can occur in scales as a result of the growth process has also been ignored so far. However, vacancies can exhibit the properties of elemental components in many respects and their precipitation can cause the formation of voids, in a manner analogous to the precipitation of other phases. Pores originating from the non-conservation of mass, caused by unequal diffusion fluxes, could occur in many of the uniform scales mentioned, except where phases are totally immiscible, but it is impossible

to define specific morphologies without more detailed information on relative diffusion rates in particular scales. Porosity may develop in association with second phase precipitation within a scale, since the particles act as preferential void nucleation sites. Grain boundaries, where vacancy concentrations are effectively higher than in the surrounding scale, may also act as preferred sites. However, this is not always the case and apparently homogeneous phases can contain large, randomly distributed pores, e.g. Cu_2S layers on Cu-Ni alloys (99). Porosity may also arise as a consequence of alloy-scale separation, scale dissociation or mechanical failure, as noted earlier. The role of vacancies and the generation of porosity during oxidation reactions has been discussed extensively in a recent series of papers (101) and mechanisms for void formation in the underlying alloy have been examined in detail by Harris (102).

OXIDATION OF MULTI-PHASE ALLOYS

So far, in the discussion emphasis has been given to cases where a common oxidation product is formed over the entire surface of the alloy, except for instances of localized breakdown referred to above. Multi-phase alloys, however, might not be anticipated to fit into this category, with each phase oxidizing, at least initially, according to its own composition. In such cases, the oxidation behavior could be considered as an approximation, as a number of different, localized reactions occurring on adjoining regions across the alloy surface. Each region will interact with its neighbors and the overall morphology will eventually consist of a complex mixture of the initial oxidation products, and the results of interactions between them. Thus, scale morphologies on more complex materials will tend to exhibit lateral variations, as determined by the local composition and microstructure of the underlying alloy. Stringer and Whittle (103) have speculated on the types of interactions which might occur, especially those relating to complex growth stress development associated with the differing oxidation rates of individual phases within the alloy. Gesmundo et al.(104) studied the behavior of Fe-Cu and Co-Cu systems representing model two phase alloy and oxide systems: both Fe and Cu and Co and Cu are virtually completely imiscible, as are their respective oxides. There are also substantial differences in oxidation rate of the two pure metals. An Fe-44% Cu alloy, however, oxidized more slowly than either of the two pure components and this was attributed to the thermodynamic destabilization of the fast growing wustite phase due to the low iron activity at the alloy/scale interface. No particular effects of growth stresses were observed. Instead,

with the exception of the preferential oxidation internally of the Fe-rich phase, the scale composition and structure were relatively uniform laterally, showing a more pronounced variation perpendicularly to the alloy surface, and suggesting that the two phase nature of the alloy does not seem to exert a strong influence in the overal oxidation behavior.

Fibre-reinforced alloys, including directionally solidified eutectic represent an increasingly important class of two-phase materials. El-Dahshan et al. (105) showed that rapid oxidation of the W-fibres in a Ni-20 Cr, W-fibre reinforced composite caused disruption of the protective Cr_2O_3 scale and considerable distortion of the matrix followed by catastrophic degradation. Figure 10 shows the oxide extrusions on the end surface of a sample, where the W-fibres were exposed: the cylindrical sides of the sample are protected by a Cr_2O_3 scale. With in-situ composites, of which Ni-Nb-Al-Cr alloys of the γ/γ'-δtype (106), and chromium carbide, tantalum carbide and niobium carbide reinforced Ni or Co-based alloys (107 ,108) have received most attention, preferential oxidation of the reinforcing fibres is not as critical. Stringer et al. (106) showed that with γ/γ'-δ alloys there was an increasing tendency to establish a continuous Al_2O_3 layer at the alloy surface as the oxidation temperature was increased in the range 800 to 1100°C. This was related to the establishment at the alloy surface, very early in the oxidation, of a continuous, single-phase $\delta(Ni_3Nb)$-free layer, at temperatures of 900°C and above. At the lowest temperature, the δ-lamellae were preferentially oxidized, with fingers of oxide extending into the metal.

In carbide-based eutectic systems (108), a critical factor affecting the formation of a protective oxide is the spacing and alignment of the carbide fibres. Small, randomly orientated fibres tend to favor the early establishment of a protective oxide, as do lower temperatures, for Cr_2O_3 - forming matrices or Cr carbide fibres. At the higher temperatures, 1000°C and above, the fibre spacing is not as critical, since invariably a carbide-depleted zone is formed between scale and bulk alloy. Formation of this fibre-denuded zone has a retarding influence on protective oxide formation, since the Cr-rich carbide fibres supply the necessary Cr: with the γ/γ'-δ alloys, the denuded zone was a pre-requisite for Al_2O_3 formation.

This supply criterion leads to the final, and perhaps most important point in relation to the oxidation of two, and multi-phase alloys, which could lead to new directions in alloy design for oxidation resistance.

This has been demonstrated (109) most dramatically in the small effect which carbon has on the overall oxidation behavior of Co-Cr alloys. Addition of carbon to a Co-25 Cr alloy produces a dispersion of the chromium-rich, $M_{23}C_6$, carbide. The presence of this carbide would thus appear to diminish the chromium content of the matrix, and hence the chromium activity of the alloy as a whole: of its 23 atoms, 18 or 19 are Cr, so that the presence of 1 wt.% C will reduce the Cr content of the matrix by 12.5 wt.%. Nevertheless, Co-Cr-C alloys with upto 2 wt.% C oxidize at virtually the same rate as a binary Co-25 Cr alloy. This is shown in Figure 11 where the ternary alloy data are plotted in terms of the effective Cr content of the matrix. The reduction in Cr activity has not affected the ability of the alloy to form a protective Cr_2O_3 layer. The reason for this is that the thermodynamic criterion for a stable Cr_2O_3 oxide is not very stringent (see earlier); the criterion that determines the establishment of an external scale relates more to the rate of transport of Cr to the surface, a criterion which can be as easily satisfied by a two phase mixture as by a single phase alloy. The important factor then, is the total atomic fraction of reactive element in the alloy, irrespective of the form in which it is present, and the ability of a two-phase alloy to form a protective oxide will not necessarily be less than that of a single phase alloy having the same overall content of the protective scale-forming element. This concept has opened up the possibility of developing oxidation-resistant alloys protected by SiO_2 and overcoming the highly adverse effects of Si on the mechanical properties, when it is present at levels of the order of those required for oxidation protection. The Si can be added to the alloy in the form of a relatively stable second phase, thereby minimizing the residual Si activity in the matrix. SiC appears to be a possible candidate, and work along these lines is currently underway (110).

ACKNOWLEDGEMENTS

Much of the work which led to this synthesis has been aided by detailed discussions over many years with various colleagues, and the contributions of Professors W. W. Smeltzer, J. Stringer and G. C. Wood and Dr. B. D. Bastow are greatefully acknowledged. The later work and the preparation of the manuscript have been supported by the Division of Materials Science, Office of Basic Energy Sciences, U. S. Department of Energy under Contract Number W-7405-ENG-48.

REFERENCES

1. P. Kofstad, High Temperature Oxidation of Metals, Wiley, New York (1966).

2. K. Hauffe, Oxidation of Metals, Plenum, New York (1965).

3. J. Benard, ed., L'Oxydation des Metaux, vols. 1 and 2, Gauthier-Villars, Paris (1962-4).

4. O. Kubaschewski and B. E. Hopkins, Oxidation of Metals and Alloys, Butterworth, London (1967).

5. G. C. Wood, Oxidation of Metals, 2, 11 (1970).

6. J. Stringer and D. P. Whittle, Rev. Int. Hautes Temp. et Refrac. 14, 6 (1976).

7. G. R. Wallwork, Repts. in Prog. in Physics 39, 401 (1976).

8. "Properties of High Temperature Alloys", ed. Z. A. Foroulis and F. S. Pettit, Electrochem. Soc. Inc., New York, N. Y. (1977).

9. "High Temperature Corrosion", Commission of European Communities, Brussels (1979).

10. "Oxidation of Metals and Alloys", ASM Monograph, Cleveland (1971).

11. "High Temperature Corrosion of Aerospace Alloys", AGARD CP 120 (1972).

12. D. P. Whittle and G. C. Wood, J. Inst. Met. 96. 115 (1968).

13. J. Moreau and J. Benard, L'Oxydation des Metaux, vol. 1, Gauthier-Villars, Paris (1962) pg. 318.

14. B. D. Bastow, G. C. Wood and D. P. Whittle, Oxidation of Metals, to be published.

15. A. D. Dalvi and D. E. Coates, Oxidation of Metals 5, 113 (1972).

16. A. D. Pelton and H. Schmalzreid, Met. Trans. 4, 1395 (1973).

17. A. U. Seybolt, J. Electrochem. Soc. 107, 149 (1960).

18. J. Croll and G. R. Wallwork, Oxidation of Metals 1, 15 (1969)

19. F. N. Rhines, Trans. AIME 137, 246 (1940).

20. J. S. Kirkaldy, Oxidation of Metals and Alloys, ASM Monograph, Cleveland (1971) pg. 101

21. J. B. Clark, Trans. Met. Soc., AIME 227, 1250 (1963).

22. C. Wagner, J. Electrochem. Soc. 99, 369 (1952).

23. D. P. Whittle, S. K. Verma and J. Stringer, Corros. Sci. 13, 247 (1973)

24. J. F. Nowak, M. Lambertine and N. C. Colson, Corros. Sci. 18, 971 (1978).

25. C. Wagner, J. Electrochem. Soc. 103, 571 (1956).

26. D. P. Whittle, D. J. Young and W. W. Smeltzer, J. Electrochem. Soc. 123, 1073 (1976).

27. C. Wagner, Corros. Sci. 9, 91 (1969).

28. R. A. Rapp, Corrosion 21, 382 (1965).

29. C. Wagner, Z. Elektrochem. 63, 773 (1969).

30. R. A. Rapp, Acta Met. 9, 730 (1961).

31. W. W. Smeltzer and D. P. Whittle, J. Electrochem. Soc. 125, 1116 (1978).

32. C. Wagner, Corros. Sci. 8, 889 (1968).

33. B. D. Bastow, D. P. Whittle and G. C. Wood, Proc. Roy. Soc. A 356, 177 (1977).

34. D. P. Whittle, B. D. Bastow and G. C. Wood, Oxid. of Metals 9, 215 (1975).

35. T. Narita and K. Nishida, Denki Kagaku 43, 433 (1975).

36. D. J. Young and W. W. Smeltzer, J. Electrochem. Soc. 123, 229 (1976).

37. G. C. Wood and T. Hodgekiess, Nature, London 211, 1358 (1966).

38. P. Mayer and W. W. Smeltzer, Oxidation of Metals Co-Fe

39. D. P. Whittle and G. C. Wood, Corros. Sci. 8 293 (1968).

40. F. S. Pettit, Trans. Met. Soc., AIME 239, 1926 (1967).

41. N. Birks and H. Rickert, J. Inst. Met. 91, 308 (1963).

42. D. P. Whittle, G. C. Wood, D. J. Evans and D. B. Scully, Acta Met. 15, 1747 (1965).

43. J. S. Armijo, Oxidation of Metals 1, 171 (1969).

44. H. Schmalzreid, Z. Physik Chem. 33, 111 (1962).

45. P. Kofstad,"Non-Stoichiometry, Diffusion and Electrical Conductivity in Binary Metal Oxides", Wiley, New York (1972).

46. W. W. Smeltzer and D. J. Young, Prog. in Solid State Chemistry 10, 17 (1975).

47. C. R. A. Catlow, W. C. Mackrodt, M.J. Norgett and A. M. Stoneham, Phil. Mag. 40, 161 (1979).

48. F. Koch and J. B. Cohen, Acta Crystalloy B25, 275 (1969).

49. N. N. Greenwood and A. T. Howe, Proc. 7th Int. Symp. Reactivity of Solids (1972).

50. B. D. Bastow, D. P. Whittle and G. C. Wood, Corros. Sci. 16, 57 (1976).

51. W. K. Chen and N. L. Petersen, J. Phys. Chem. Solids 34, 1093 (1973).

52. Von G. Schweir, R. Dieckmann and H. Schmalzried, Ber. Bunsenges. Physik, Chem. 77, 402 (1973).

53. G. C. Wood, I. G. Wright and J. M. Ferguson, Corros. Sci. 5, 645 (1965).

54. A. D. Dalvi and D. E. Coates, Oxidation of Metals 3, 303 (1971).

55. T. Narita and K. Nishida, Nippon Kink. Gakk. 29, 1152 (1975).

56. A. D. Dalvi and W. W. Smeltzer, J. Electrochem. Soc. 121, 386 (1974).

57. P. Mayer and W. W. Smeltzer, J. Electrochem. Soc. 119, 626 (1972).

58. P. Mayer and W. W. Smeltzer, J. Electrochem. Soc. 121, 538 (1974).

59. T. Narita and K. Nishida, Denki Kagaku, 43, 433 (1975).

60. D. J. Young, P. Mayer and W. W. Smeltzer, J. Electrochem. Soc. 121, 889 (1974).

61. D. J. Young and W. W. Smeltzer, J. Electrochem Soc. 123, 229 (1976)

62. R. Dieckmann, Z. fur physik. Chemic NF 107, 189 (1977).

63. F. Fryt, Oxidation of Metals 10, 311 (1976).

64. D. P Whittle, F. Gesmundo and F. Viani, Oxid. of Metals, to be published.

65. F. Gesmundo and F. Viani, J. Electrochem. Soc., to be published.

66. C. M. Osburn and R. W. Vest, J. Phys. Chem. Solids 32, 1343 (1971).

67. G. Koel and P. Jennings, Oxid. Met. 5, 185 (1972).

68. D. P. Whittle, F. Gesmundo and F. Viani, to be published.

69. R. Dieckmann and H. Schmalzried, Ber. Bunsenges Physik Chem. 79, 1108 (1975).

70. D. J. Young, T. Narita and W. W. Smeltzer, J. Electrochem. Soc. 127, 679 (1980).

71. G. C. Wood, I. G. Wright, T. Hodgkiess and D. P. Whittle, Werk, u. Korr. 21, 900 (1970).

72. J. D. Hodge, J. Electrochem. Soc. 125, 55C (1978).

73. Y. Shida, F. H. Stott, D. P. Whittle and G. C. Wood, Oxidation of Metals, to be published.

74. D. P. Whittle and G. C. Wood, Br. Corros. J. 3, 294 (1980).

75. B. Chattopadhyay and G. C. Wood, Oxid. Met. 2, 373 (1970)

76. S. K. Verma, G. E. Reynaud and R. A. Rapp, Oxid. Met., to be published.

77. C. S. Giggins and F. S. Pettit, Trans. Met. Soc., AIME 245, 2509 (1969).

78. C. E. Lowell, Oxid. Met. 5, 205 (1972).

79. C. Wagner, Corros. Sci. 5, 751 (1965).

80. H. W. Pickering, J. Electrochem. Soc. 119, 641 (1972).

81. F. A. Golightly, G. C. Wood and F. H. Stott, Oxid. Metals 14, 217 (1980).

82. F. H. Stottt and G. C. Wood, Corros. Sci. 11, 799 (1971).

83. G. N. Irving, J. Stringer and D. P. Whittle, Corrosion 33, 56 (1977).

84. G. N. Irving, J. Stringer and D. P. Whittle, Oxid. Met. 9, 427 (1975).

85. J. Stringer, private communication

86. A. Green, M. Eng. thesis, University of Liverpool (1975).

87. G. W. Roper and D. P. Whittle, Met. Sci. J. Jan. 14 (1980).

88. D. P. Whittle and J. Stringer, Phil. Trans. Roy. Soc., London A295, 309 (1980).

89. D. P. Whittle, M.E. El Dahshan and J. Stringer, Corros. Sci. 17, 879 (1977).

90. J. Stringer and A. Z. Hed, Oxid. Met. 3, 571 (1971).

91. H. H. Davis, H. C. Graham and I. A. Kvernes, Oxid. Met. 3, 431 (1971).

92. J. Stringer, B. A. Wilcox and R. I. Jaffee, Oxidation Met. 5, 11 (1972).

93. I. M. Allam, D. P. Whittle and J. Stringer, Oxid. Met. 12, 35 (1978).

94. I. G. Wright, B. A. Wilcox and R. I. Jaffee, Oxid. Met. 9, 275 (1975).

95. H. M. Flower and B. A. Wilcox, Corros. Sci. 17, 253 (1977).

96. D. P. Whittle, Corros. Sci. 12, 869 (1972).

97. H. C. Cowen and S. J. Webster, Proc. BNES Conf., Reading (1974).

98. F. A. Golightly, F. H. Stott and G. C. Wood, Oxid, Met. 10, 163 (1973).

99. B. D. Bastow and G. C. Wood, Corros. Sci. 18, 275 (1978).

100. D. P. Whittle, Oxid. Met. 4, 171 (1972).

101. R. E. Smallman and J. E. Harris (eds.), Proc. Conf. "Vacancies 76", (The Metals Society, London, 1977) session IV, pp. 187-222.

102. J. E. Harris, Acta Met. 26, 1033 (1978).

103. J. Stringer, P. Corkish and D. P. Whittle, "Stress Effects and the Oxidation of Metals", J. Cathcart (ed.) ASM, (1975).

104. F. Gesmundo, P. Nanni and D. P. Whittle, J. Electrochem. Soc. 127, 1773 (1980).

105. M. E. El Dahshan, D. P. Whittle, and J. Stringer, Oxid. Met. 9, 45 (1975).

106. J. Stringer, D. M. Johnson and D. P. Whittle, Oxid. Met. 12, 257 (1978).

107. F. H. Stott, G. C. Wood and J. G. Fountain, Oxid. Met. 14, 31 (1980).

108. D. M. Johnson, D. P. Whittle and J. Stringer, Tech. Rept. No. AFML-TR-78-137, Wright Patterson AFB, Ohio (1978).

109. M. E. El Dahshan, D. P. Whittle and J. Stringer, Cobalt 3, 86 (1974).

110. J. Stringer, D. P. Whittle, I. G. Wright, M. E. El Dahshan and V. Nagarajan, to be published.

FIGURE CAPTIONS

Figure 1 - Schematic alloy oxidation kinetics showing different stages in alloy oxidation.

Figure 2 - Schematic representation of the Ni-Cr-O equilibrium diagram between 900-1100°C.

Figure 3 - Schematic phase diagram and equilibrium oxygen pressure diagram for noble metal alloys showing typical diffusion paths and concentration profiles.

Figure 4 - Schematic phase diagram and equilibrium oxygen pressure diagram for systems in which the oxide phases are completely miscible. Typical diffusion paths and concentration profiles through alloy and scale are also shown.

Figure 5 - The variation of the normalized rate constant, $K/K_{B(x)}$, with alloy composition demonstrating the effect of different degrees of selective oxidation of the component B for the limiting cases:

D_{all}/D_B^O	$\delta(\Delta G)$ = 125.6	20.9 KJ/mol
∞	curve 1	curve 2
0	curve 3	curve 4

Figure 6 - Schematic phase diagram and equilibrium oxygen pressure diagram for systems in which the oxides and partially miscible.

Figure 7 - A comparison between experimental and theoretical cation profiles and growth rate contants for scales formed on Ni-Co alloys at 1000°C (50).

Figure 8 - Oxidation rates of Fe-, Ni-, and Co-Cr alloys as a function of composition at 1000°C (71).

Figure 9 - Schematic diagram illustrating how dispersed oxide particles, by acting as nucleation sites for the first-formed oxide, accelerate the approach to steady state and reduce the amount of Ni-containing oxides in the oxidation of Ni-20Cr (a) without and (b) with dispersed oxide particles (92).

Figure 10 - Oxidation of W-fibre reinforced Ni-20Cr alloys showing rapid oxidation of the fibres causing break-up of the matrix.

Figure 11 - Comparison of the parabolic rate constants for the oxidation at 1000°C of Co-25Cr-C and Co-Cr alloys. Data points for C-containing alloys have been plotted as effective Cr contents (109). Data for binary alloys are from Wood et al. (71).

Figure 1

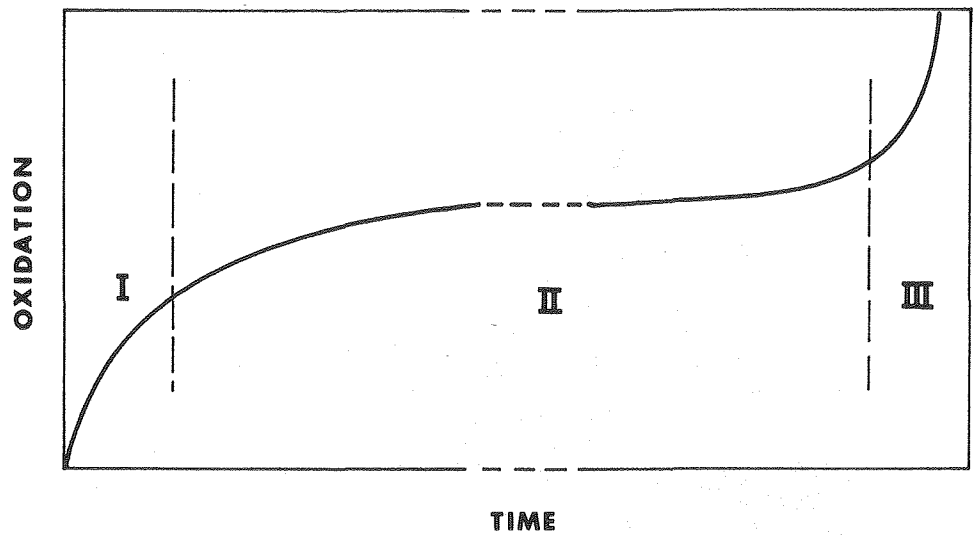

I: TRANSIENT STAGE: RATIO OF CATIONS IN SCALE APPROXIMATELY SAME AS THAT IN ALLOY.

II: STEADY STATE: OXIDE MORPHOLOGY AND COMPOSITION DETERMINED BY DIFFUSION AND THERMODYNAMICS OF OXIDE/ALLOY SYSTEM.

III: BREAKAWAY: INITIATED BY MECHANICAL FACTORS: EVENTUALLY SCALE CONTAINS ALLOYING COMPONENTS IN ORIGINAL ALLOY RATIO.

XBL 812-8141

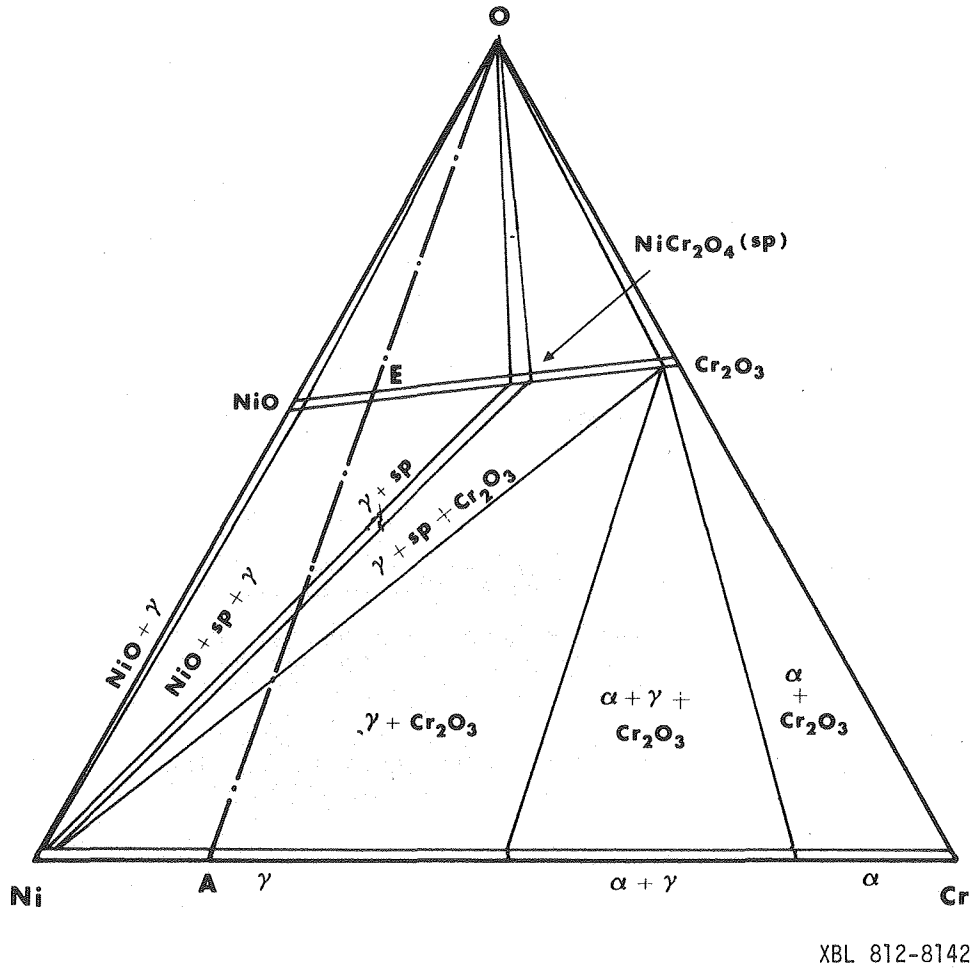
O
$NiCr_2O_4$(sp)
Cr_2O_3
E
NiO
γ + sp
γ + sp + Cr_2O_3
NiO + γ
NiO + sp + γ
γ + Cr_2O_3
$\alpha + \gamma +$ Cr_2O_3
α + Cr_2O_3
Ni
A
γ
$\alpha + \gamma$
α
Cr
XBL 812-8142

Figure 2

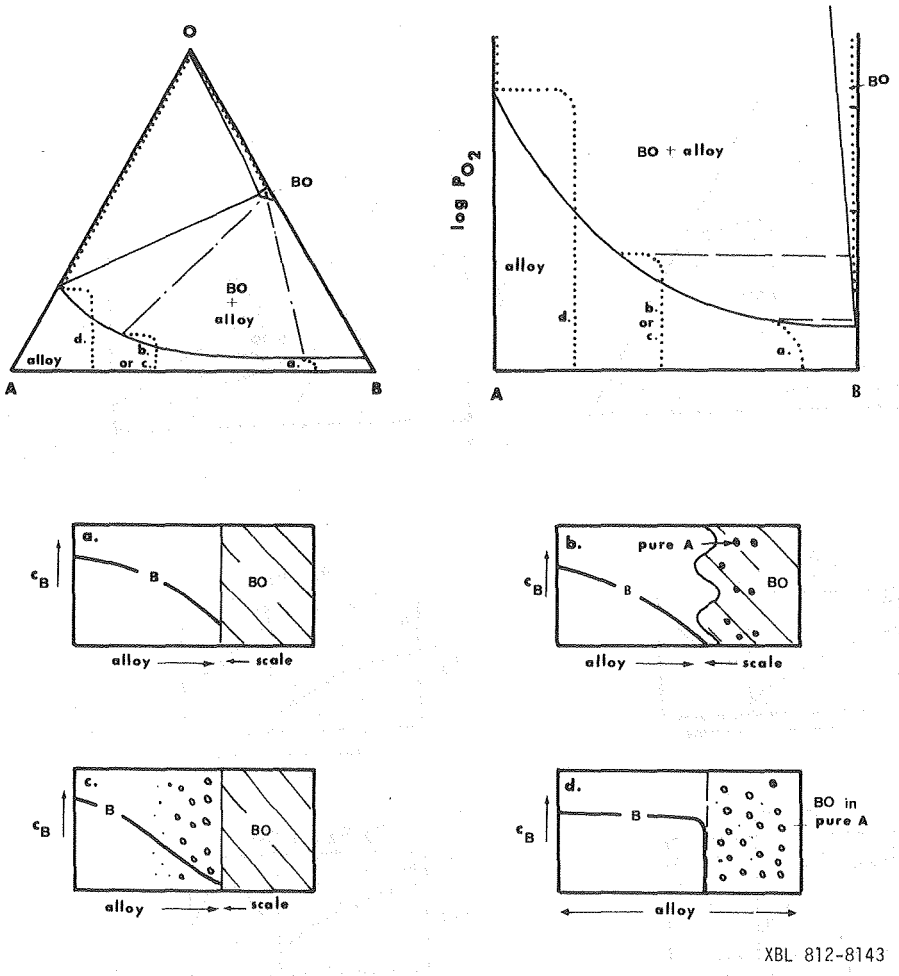
O
BO
BO
+
alloy
alloy
d.
b.
or c.
a.
A
B
log P_{O_2}
BO + alloy
BO
alloy
d.
b.
or
c.
a.
A
B
a.
c_B
B
BO
alloy
scale
b.
pure A
c_B
B
BO
alloy
scale
c.
c_B
B
BO
alloy
scale
d.
c_B
B
BO in
pure A
alloy
XBL 812-8143

Figure 3

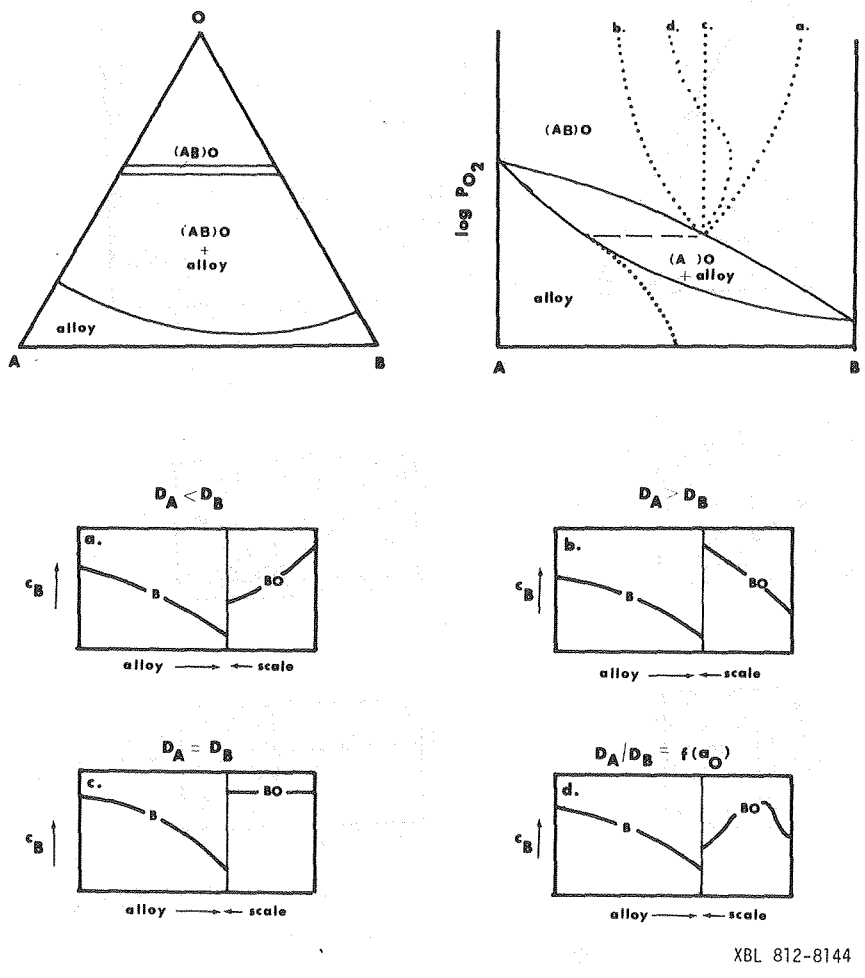
O
(AB)O
(AB)O
+
alloy
alloy
A
B
b.
d.
c.
a.
(AB)O
log P_{O_2}
(A)O
+ alloy
alloy
A
B
$D_A < D_B$
a.
c_B
B
BO
alloy
scale
$D_A > D_B$
b.
c_B
B
BO
alloy
scale
$D_A = D_B$
c.
c_B
B
BO
alloy
scale
$D_A/D_B = f(a_O)$
d.
c_B
B
BO
alloy
scale
XBL 812-8144

Figure 4

Figure 5

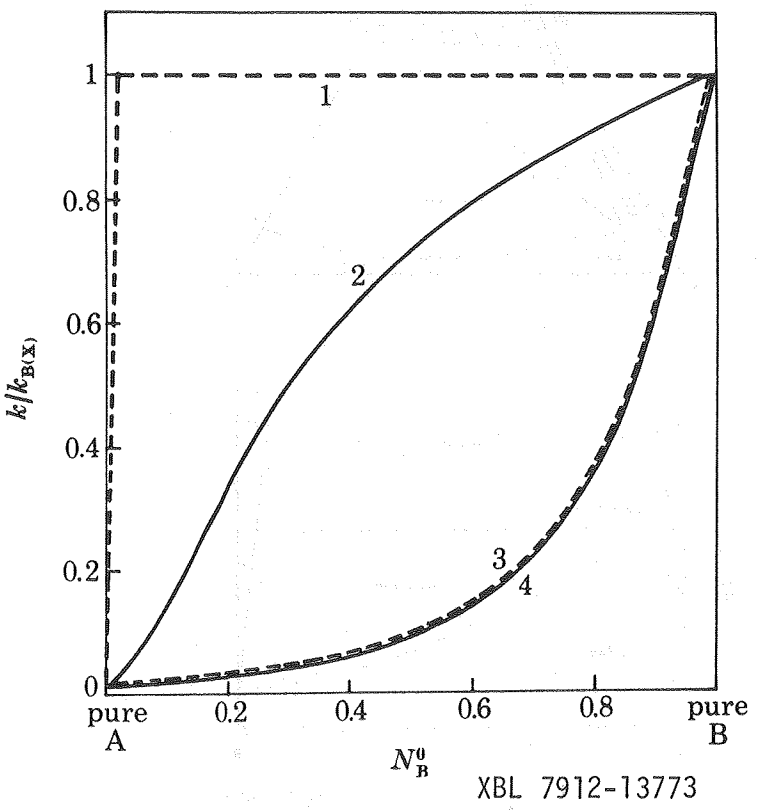
1
0.8
0.6
0.4
0.2
0
$k/k_{B(X)}$
1
2
3
4
pure
A
0.2
0.4
0.6
0.8
pure
B
N_B^0
XBL 7912-13773

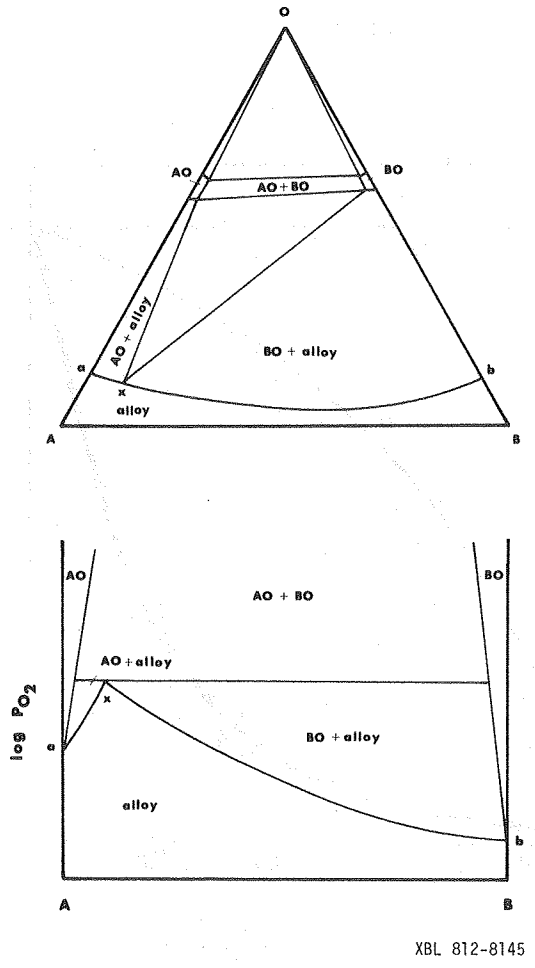
O
AO
BO
AO + BO
AO + alloy
BO + alloy
a
x
b
alloy
A
B
AO
BO
AO + BO
AO + alloy
log P_{O_2}
x
a
BO + alloy
alloy
b
A
B
XBL 812-8145

Figure 6

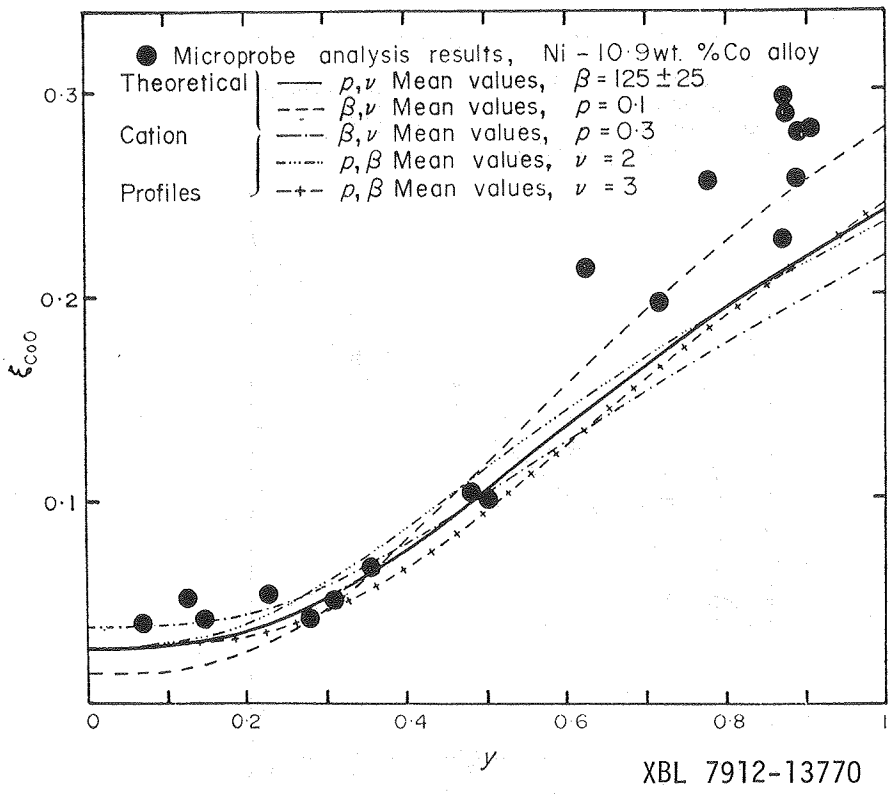
Microprobe analysis results, Ni - 10·9wt. %Co alloy
Theoretical
Cation
Profiles
p,ν Mean values, β = 125 ± 25
β,ν Mean values, p = 0·1
β,ν Mean values, p = 0·3
p,β Mean values, ν = 2
p,β Mean values, ν = 3
0·3
0·2
0·1
ξCoO
0
0·2
0·4
0·6
0·8
1
y
XBL 7912-13770

Figure 7

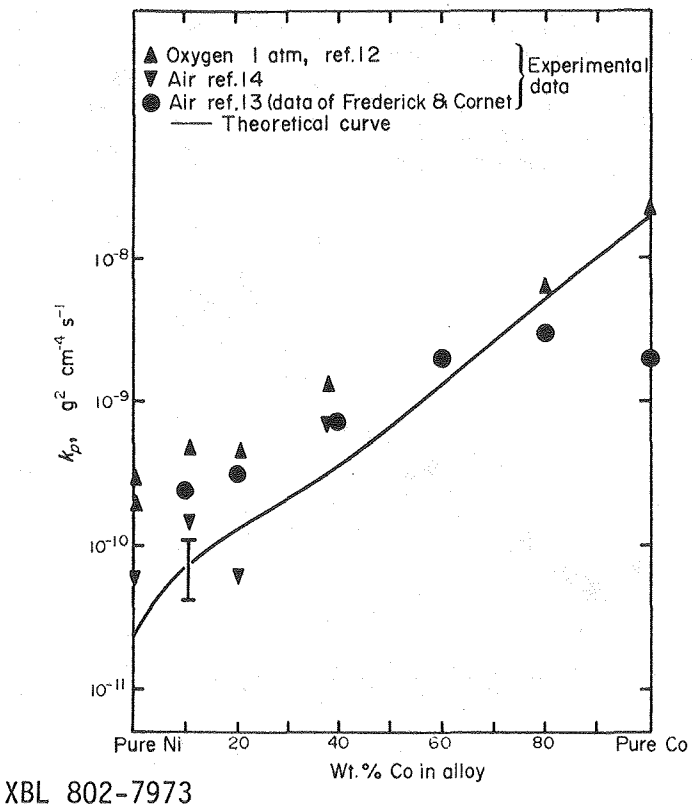

XBL 802-7973

Figure 7 (cont'd)

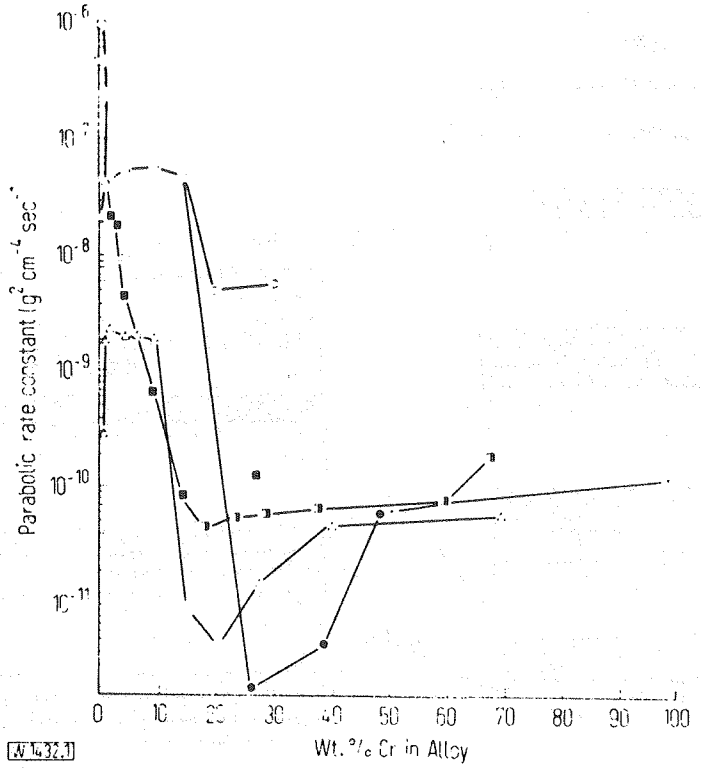
Parabolic rate constant (g² cm⁻⁴ sec⁻¹
10⁻⁶
10⁻⁸
10⁻⁹
10⁻¹⁰
10⁻¹¹
0
10
30
40
50
60
70
80
90
100
Wt. % Cr in Alloy
W 1432.1

Figure 8

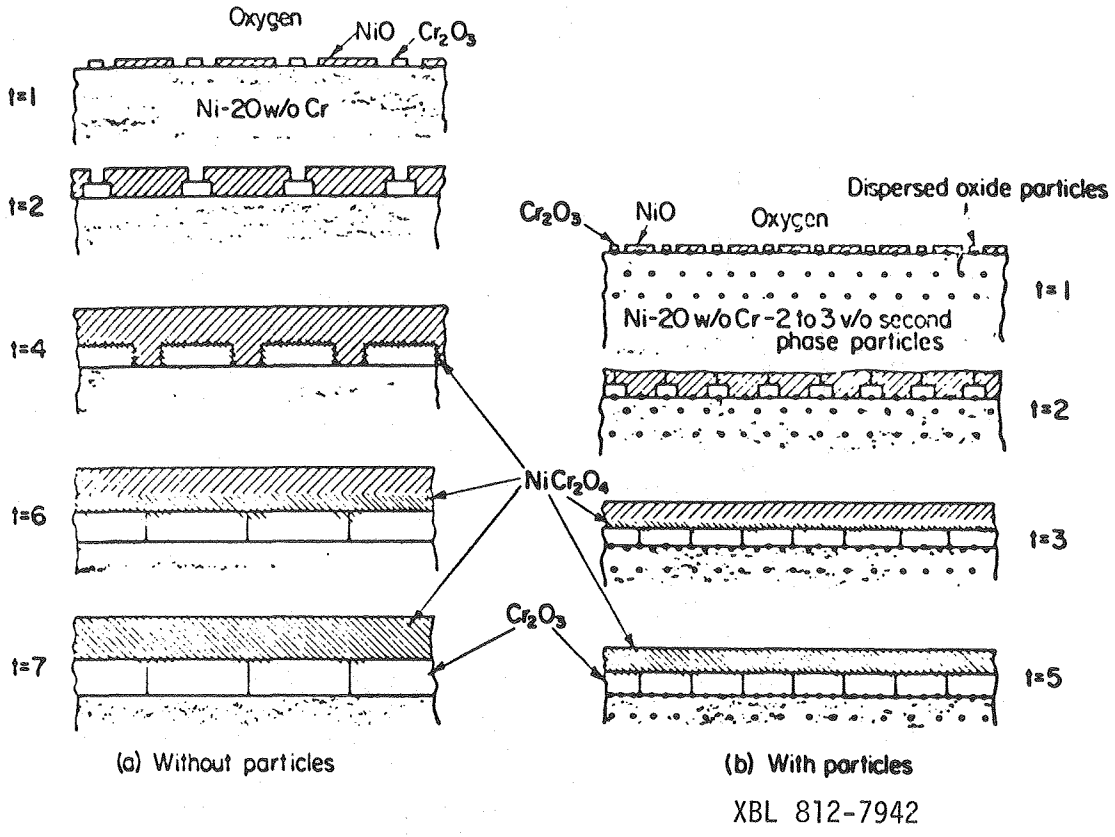
Oxygen
NiO
Cr_2O_3
t=1
Ni-20w/o Cr
t=2
t=4
t=6
t=7
$NiCr_2O_4$
Cr_2O_3
(a) Without particles
Cr_2O_3
NiO
Oxygen
Dispersed oxide particles
Ni-20 w/o Cr-2 to 3 v/o second phase particles
t=1
t=2
t=3
t=5
(b) With particles
XBL 812-7942

Figure 9

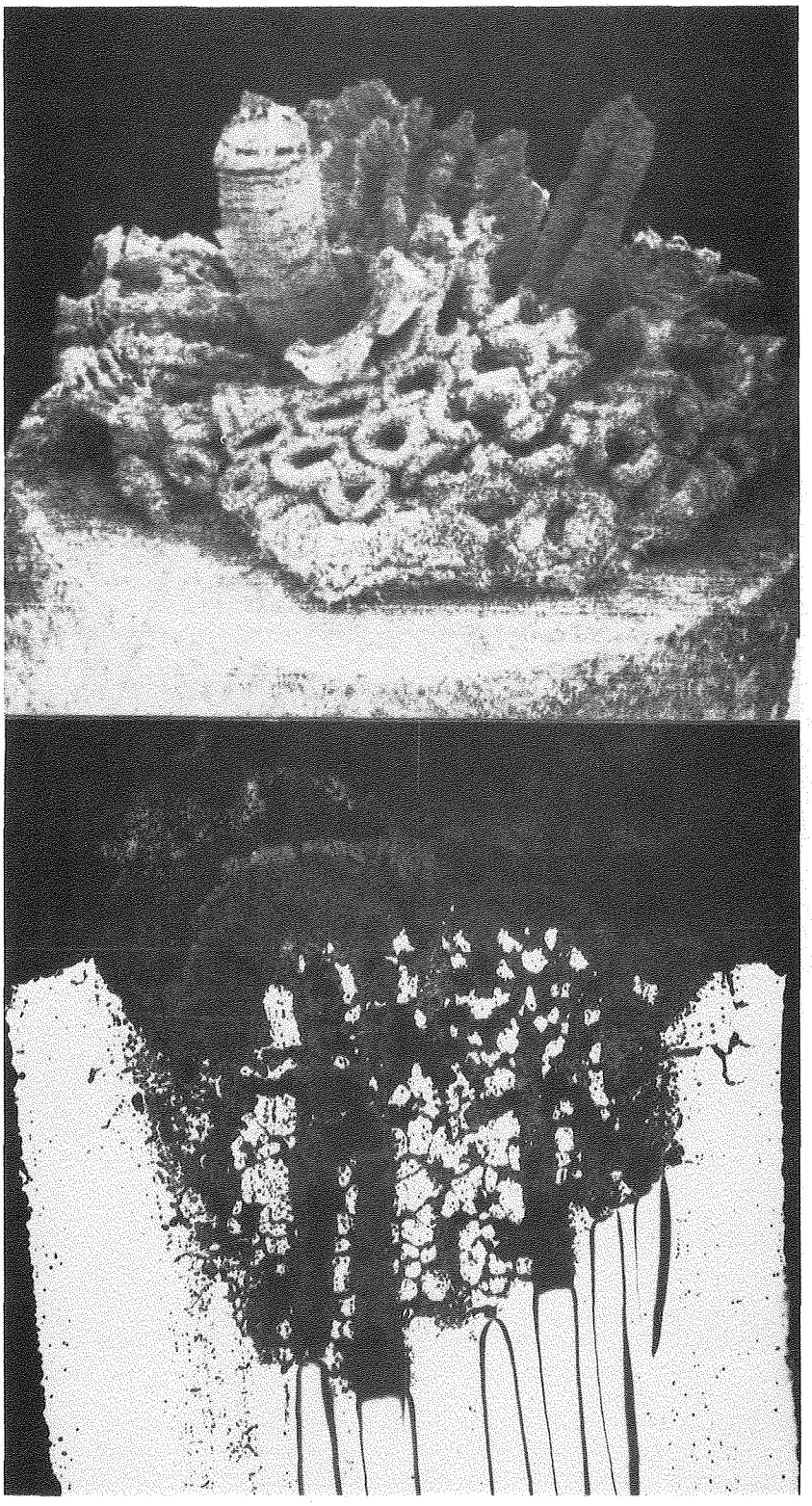

Figure 10 XBB 811-1916

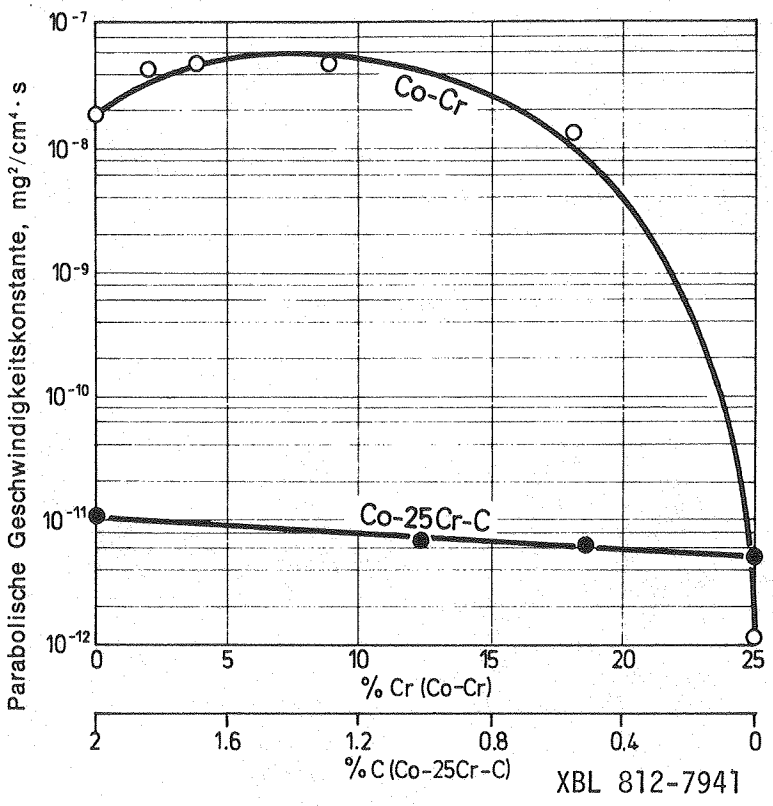
Parabolische Geschwindigkeitskonstante, mg²/cm⁴ · s
10⁻⁷
10⁻⁸
10⁻⁹
10⁻¹⁰
10⁻¹¹
10⁻¹²
Co-Cr
Co-25Cr-C
0
5
10
15
20
25
% Cr (Co-Cr)
2
1.6
1.2
0.8
0.4
0
% C (Co-25Cr-C)
XBL 812-7941

Figure 11